View metadata, citation and similar papers at core.ac.uk

brought to you by CORE

provided by Kanazawa University Repository for Academic Resources

Fossil tubeworms link coastal uplift of the northern Noto Peninsula to rupture of the Wajima-oki fault in AD 1729

著者	Hamada Masaaki, Hiramatsu Yoshihiro, Oda Mitsuhiro, Yamaguchi Hiroyuki
journal or publication title	Tectonophysics
volume	670
page range	38-47
year	2016-02-22
URL	http://hdl.handle.net/2297/45094

doi: 10.1016/j.tecto.2015.12.019

Fossil tubeworms link coastal uplift of the northern Noto Peninsula to rupture of the Wajima-oki fault in AD 1729

Masaaki Hamada

Graduate School of Natural Science and Technology, Kanazawa University, Kanazawa, Japan

Yoshihiro Hiramatsu

School of Natural System, College of Science and Engineering, Kanazawa University, Kanazawa, Japan

Mitsuhiro Oda

Hokuriku Electric Power Co., Ltd., Toyama, Japan

Hiroyuki Yamaguchi

Natural Consultant Co., Ltd., Nonoichi, Japan

Corresponding author: M. Hamada, Graduate School of Natural Science and Technology, Kanazawa University, Kakuma, Kanazawa 920-1192, Japan (hamada@hakusan.s.kanazawa-u.ac.jp)

KEYWORDS: Coseismic crustal movement, Active fault, Intertidal sessile organisms, Radiocarbon dating, Fault model

Highlights

· Carbon dating of sessile organisms indicates uplift time of coastal area of Japan.

· Marine fault activity in 18th century connected to coastal uplift of peninsula.

· Earthquake damage records are consistent with fault model from uplift estimates.

Abstract

The active fault zone on the seafloor off the northern coast of the Noto Peninsula of central Japan is divided into four segments from west to east: Monzen-oki, Saruyama-oki, Wajima-oki, and Suzu-oki. To examine the latest event that occurred in these segments, we investigated the dates and elevations of fossilized intertidal tubeworms along the northern coast of the Noto Peninsula, located on the hanging-wall sides of the faults, using radioactive carbon dating and global positioning measurements. For each fossil, we calculated the difference between the past and present elevation, thereby estimating the elevation of the sea level at the date of the fossil, using a curve for sea level change. This calculation provided us with the elevation change at each site. The radiocarbon dates of the fossils, together with the elevation changes, revealed that the coastal emergence probably occurred between 1600 and 1800 AD. This area of coastal emergence lies adjacent to active faults within the Wajima-oki segment. A model for rectangular faults with three fault planes and a moment magnitude of 6.6 for the Wajima-oki segment reproduced the observed pattern of coastal emergence well. Only one damaging earthquake, that in 1729, is known to have occurred in this part of the northern Noto Peninsula between 1600 and 1800 AD, and there has not been one since 1800 AD. The slip distribution of the earthquake predicted by the model is consistent with the distribution of shaking-related damage documented in 1729. We conclude that rupture of the Wajima-oki segment caused the 1729 earthquake.

1. Introduction

The faulting history of active faults is one of the key types of information needed to explain regional tectonics and geomorphological evolution. Geophysical and geological surveys data, including paleogeodetic data, examined along with historical documents, can reveal details of the faulting history, such as the date of the latest event, the recurrence interval, and the crustal deformation. For a large fault system with several segments, it is important to examine the faulting history of each segment and the interactions between the segments. However, there are several problems to be addressed in comparing geophysical and geological observations with historical data. For example, a historical document may describe severe seismic damage in an area, but there may be no source location and/or source fault that has been identified as the cause of that damage, even though there are active faults in or around the area. Therefore, to achieve a comprehensive understanding of regional tectonics, it is important to obtain geophysical and geological evidence of historical earthquakes and construct a fault model that is consistent with geophysical and geological observations and historical data.

Holocene marine terraces, intertidal organisms, and wave-cut benches are useful markers of the faulting history of marine active faults (e.g., Yamaguchi and Ota, 2004; Hsieh and Rau, 2009; Ramos and Tsutsumi, 2010). Many studies have been conducted on tectonic uplift using *Pomatoleios kraussii* (hereinafter termed *P. kraussii*) assemblages in Japan (Kayanne et al., 1987; Nishihata et al., 1988; Maemoku, 1988; Shishikura et al., 2008). *P. kraussii* forms colonial zonation or patches of calcareous tubes that can only survive within a narrow range of the mid-tidal zone on rocky coasts, and the upper limit of the range corresponds to the mean sea level (Imajima, 1979; Miura and Kajihara, 1983, 1984; Kayanne et al., 1987). The emerged *P. kraussii*

assemblages are therefore excellent indicators of historical mean sea levels. Sampling of *P. kraussii* along coastlines can reveal pseudo-two-dimensional coseismic crustal deformation associated with a particular paleo-earthquake, in contrast to one-dimensional or point-based paleoseismic trench investigation across a fault.

The Noto Peninsula, located in the backarc region of the Japanese islands, is an area with developed marine terraces (Ota and Hirakawa, 1979). The Noto Peninsula is one of Japan's foremost areas of marine fault activity, with an uplift rate of more than 1 mm/yr. However, the relationship between this fault activity and the earthquake history of the area has not been established, even though historical documents show that a damaging earthquake occurred in 1729 in the area of the Noto Peninsula (Usami, 2003). Recently, an active fault zone with several segments has been identified on the seafloor off the Noto Peninsula (Inoue and Okamura, 2010), but little is known about the activity of these active faults.

In this paper, we present estimates of the vertical displacements along the northern coast of the Noto Peninsula, obtained using the elevations and ages of intertidal sessile organisms. We also identify the latest active marine fault event, based on vertical displacement data, and we present a source model of the latest event. Finally, we discuss the relationship between the latest event, historical records, and the marine fault activity along the coast through the Late Pleistocene.

2. Tectonic and geologic setting

2.1. Geology and geomorphology

Jurassic granites, Oligocene igneous rocks, Miocene volcanic rocks, and sedimentary rocks, and Pleistocene terrace deposits are distributed along the northern part of the Noto Peninsula (Ozaki, 2010). Around the Noto Peninsula, normal faults were formed

by extension tectonics during the expansion of the Sea of Japan in the Early Miocene, and these normal faults were converted into reverse faults as a result of north–south compressive stress during the Late Miocene (Okamura, 2002; Sato et al., 2007). Normal faults trending NE–SW, reverse faults trending ENE–WSW to E–W, and reverse faults trending NNE–SSW to NE–SW developed (Ozaki, 2010) (Fig. 1).

Pleistocene marine terraces along the coast, which are located on the uplift areas of these segments, indicate the upheaval in the coastal area through the late Quaternary (Ota and Hirakawa, 1979). The study area is topographically divided into several blocks, and each block is tilted in the southeastern direction (Yoshikawa and Yazawa, 1955). Differences in elevation of the Late Pleistocene marine terraces have been found at the boundaries of the blocks (Ota and Hirakawa, 1979) (Fig. 1).

Inoue and Okamura (2010) conducted a high-resolution multi-channel seismic survey of profiles, spaced at intervals of 1.8 km and oriented nearly perpendicular to the active marine faults off the northern coast of the Noto Peninsula, and reported a two-dimensional seismic velocity structure along each profile. Several two-dimensional seismic velocity structures illustrated a clear reverse fault structure dipping to the southeast, although others did not, indicating horizontal continuity among active marine faults. Inoue and Okamura (2010) divided the active fault zone into four segments from west to east—Monzen-oki, Saruyama-oki, Wajima-oki, and Suzu-oki—based on gaps in the fault traces of the active fault zone (Fig. 1).

2.2. Historical earthquakes

The past seismicity of large earthquakes in Japan has been investigated on the basis of damage distributions described in historical records (e.g., Usami, 2003). Usami (2003) reported the distribution of collapsed building ratios associated with an

earthquake (the 1729 Noto–Sado earthquake) along the coast south of the Wajima-oki segment, based on historical documents from 1729, and estimated the magnitude of this earthquake to be 6.6–7.0, based on the distribution. However, the source fault of this event has not been identified.

The epicenter of the 1993 Noto Hanto-oki earthquake (M_{JMA} 6.6) was located 10 km north of the Suzu-oki segment, but the relation between the 1993 event and the Suzu-oki segment is not clear (Fig. 1).

The eastern half of the Monzen-oki segment, which was illustrated by fault traces by Katagawa et al. (2005), caused the 2007 Noto Hanto earthquake (M_{JMA} 6.9) (Inoue and Okamura, 2010) (Fig. 1). A focal mechanism of the 2007 Noto Hanto earthquake was a reverse fault with a right–lateral slip and a compression axis with a NW–SE orientation (NIED, 2007). The distribution of the aftershocks indicates that the dip and strike of the source fault were a high angle (60°) and nearly NE–SW, respectively (Sakai et al., 2008). The coseismic crustal deformation caused by the 2007 earthquake has been estimated based on geodetic measurements, including measurements made using a global positioning system (GPS) (Ozawa et al., 2008), synthetic aperture interferometry (InSAR) (Ozawa et al., 2008), and airborne LiDAR (Nohara et al., 2007). These findings are consistent with the estimated uplift based on the distribution of supra-, mid-, and infra-littoral organisms (Awata et al., 2008; Hiramatsu et al., 2008; Shishikura et al., 2009).

3. Methods

3.1. Measurement of the elevation of sessile organisms

The elevations of intertidal sessile organisms were measured using GPS (LEGACY-H/GD, TOPCON, Japan). We used the GPS-based control stations of the

Geospatial Information Authority of Japan near the survey area for the reference point of the GPS. Elevations were determined with reference to the mean sea level of Tokyo Bay (elevation 0 m). Because the absolute value of the coseismic crustal deformation caused by the 2007 Noto Hanto earthquake in the survey area is estimated to be less than 4 cm (Hiramatsu et al., 2008), the coseismic crustal deformation of this earthquake does not affect our observations.

We used a sea level change curve to determine the difference in elevation between the past and present sea levels, because the sea level has changed over time as a result of climate change. Unfortunately, the results of previous studies on sea level change curves have not proven to be adequate for the study area. Therefore, we used the millennium sea level change for the Northern Hemisphere, based on climate change data (Moberg et al., 2005) reported by Grinsted et al. (2009).

3.2. Dating of emergent organisms

The emergent organisms were dated by the Institute of Accelerator Analysis, Ltd. and Beta Analytic, Inc., using the accelerator mass spectrometry (AMS) ^{14}C method. The conventional age results were calibrated with respect to the calendar year using the Marine09 data sets (Reimer et al., 2009), and the median and two-sigma probability range were calculated using OxCalv4.1 (Bronk Ramsey, 2009) as the calibration program. Because the difference between the global mean and the local reservoir effect (ΔR) has not been reported for this area, we calculated the calendar year assuming $\Delta R = 0$. Shishikura et al. (2009) adopted $\Delta R = -25 \pm 28$ years for a survey of the western coast of the Noto Peninsula, based on survey results for a different region in Japan. If we use this value for ΔR, the difference in the vertical displacement is estimated to be 0.06 m at most and does not alter the observations presented in this paper.

3.3. Fault modeling

To test that the fault movement of the Wajima-oki segment caused the uplift estimated by the elevations of the *P. kraussii* assemblages, we constructed a fault model of the segment using the nonlinear inversion method proposed by Matsu'ura and Hasegawa (1987).

4. Ages and locations of sessile organisms

We chose *P. kraussii* from among various intertidal sessile organisms for use as a sea-level indicator, reconstructed emergent shorelines, and investigated the occurrence of this organism along a rocky coast within a range of 60 km of the northern Noto Peninsula (Fig. 1). The field measurements were obtained between April 2010 and November 2011.

We found 14 samples of fossilized *P. kraussii* assemblages at eight sites and some modern samples. These assemblages were found mainly along a rocky coast that extends from a precipitous wave-cut cliff. Figure 2b shows an example of the distribution of the fossilized *P. kraussii* assemblages at Site C. The elevations and radiocarbon dates of the samples are summarized in Figure 3 and Table 1.

4.1. Modern assemblages

We measured the elevation of modern *P. kraussii* assemblage at five sites. The *P. kraussii* assemblage at Site A is distributed within the elevation range of 0.23–0.31 m. The elevation ranges of the modern assemblage at Sites C, E, and G are 0.15–0.36 m, 0.22–0.36 m, and 0.18–0.30 m, respectively (Fig. 2a, Fig. 3). Site I is located approximately 7 km from the nearest part of the Suzu-oki segment and is approximately 8 km east of Site H (Fig. 1). A modern *P. kraussii* assemblage is observed in the calcareous tubes distributed over an elevation range of 0.35–0.58 m along a crack at the retreat point of the basal portion of the wave-cut notch at Site I. The assemblage is a few

millimeters thick.

4.2. Fossil assemblages

4.2.1. Site A

Site A is located in the coastal area corresponding to the boundary between the Monzen-oki and Saruyama-oki segments. A *P. kraussii* assemblage with a thickness of approximately 3 cm is distributed over an elevation range of 0.2–0.35 m along the rampart of the tip of the wave-cut bench. Applying the ^{14}C method, a calendar year in the range of 1550–1678 AD (± 2σ) with a median of 1631 AD was obtained for the inside (the part facing the bedrock) of the assemblage distributed at an elevation of 0.35 m.

4.2.2. Site B

Site B is located in the coastal area corresponding to the boundary between the Saruyama-oki and Wajima-oki segments. Two *P. kraussii* assemblages are distributed at two levels along a crack on the wave-cut bench. The lower assemblage is distributed in the elevation range of 0.0–0.42 m. The upper assemblage is distributed in the elevation range of 0.54–0.71 m. These two assemblages are only a few millimeters thick. Using the ^{14}C method, we obtained a calendar-year range of 1186–1291 AD (± 2σ) with a median of 1244 AD for the upper assemblage (B1, 0.71 m) and a calendar-year range of 1476–1630 AD (± 2σ) with a median of 1535 AD for the lower assemblage (B2, 0.42 m).

4.2.3 Site C

Site C is located in the closest coastal area to the western part of the Wajima-oki segment. Two *P. kraussii* assemblages are distributed over two levels along a crack developing on a wave-cut notch. The lower assemblage is distributed at an elevation of 0.36 m. The upper assemblage is intermittently distributed over an elevation range of

1.07–1.59 m. These assemblages are only a few millimeters thick. The ^{14}C method was used to estimate a calendar-year range of 1080–1239 AD (± 2σ) with a median of 1175 AD for sample C1, a calendar-year range of 1525–1660 AD (± 2σ) with a median of 1594 AD for sample C2 in the upper assemblage (top: C1, 1.59 m; bottom: C2, 1.07 m), and a calendar-year range of 1708 AD to the present (± 2σ) with a median of 1819 AD for sample C3 in the lower assemblage (C3, 0.36 m).

4.2.4 Site D

Site D is located in the coastal area corresponding to the central part of the Wajima-oki segment. Around the site, a sandy beach extends from the Holocene-emerged shoreline topography and alluvial plain. The development of wave-cut benches is poor in this area. A *P. kraussii* assemblage is distributed at an elevation of 1.05 m along a crack in the bedrock. Applying the ^{14}C method, a calendar-year range of 1139–1280 AD (± 2σ) with a median of 1214 AD was obtained for the assemblage.

4.2.5 Site E

Site E is located in the coastal area corresponding to the boundary between the central and eastern parts of the Wajima-oki segment. A *P. kraussii* assemblage approximately 2 cm thick is distributed at an elevation of 0.85 m, along a crack in the roof point of the wave-cut notch. Applying the ^{14}C method, a calendar-year range of 1235–1325 AD (± 2σ) with a median of 1286 AD was estimated.

4.2.6 Site F

Site F is located in the coastal area corresponding to the eastern part of the Wajima-oki segment. A *P. kraussii* assemblage is distributed over an elevation range of 0.76–1.04 m along a crack in the bedrock. The assemblage is only a few millimeters thick. We estimated ages for the top of the assemblage (F1, 1.04 m) and the bottom of

the assemblage (F2, 0.76 m) using the ^{14}C method and obtained a calendar-year range of 1168–1280 AD (± 2σ) with a median of 1226 AD for sample F1 and a calendar-year range of 1360–1478 AD (± 2σ) with a median of 1433 AD for sample F2.

4.2.7 Site G

Site G is located in the coastal area corresponding to the boundary between the Wajima-oki and Suzu-oki segments. A *P. kraussii* assemblage approximately 1 cm thick is distributed over an elevation range of 0.28–0.59 m along a crack in the basal portion of the wave-cut notch. We estimated ages for the top (G1, 0.59 m) and bottom (G2, 0.28 m) of the assemblage using the ^{14}C method and obtained a calendar-year range of 1520–1686 AD (± 2σ) with a median of 1609 AD for sample G1 and a calendar-year range of 1693 AD to the present (± 2σ) with a median of 1800 AD for sample G2.

4.2.8 Site H

Site H is located in the coastal area near the west end of the Suzu-oki segment. A *P. kraussii* assemblage approximately 5 cm thick is distributed over an elevation range of 0.69–0.92 m. The thickness increases near the bottom of the distribution. The assemblage is distributed along a crack at the retreat point of the basal portion of a mushroom rock. Using the ^{14}C method, the calendar-year ranges and medians for the top of the assemblage (H1, 0.92 m) and bottom of the assemblage (H2, 0.69 m) were estimated to be 1186–1341 AD (± 2σ) and 1276 AD, respectively, for sample H1 and 1332–1473 AD (± 2σ) and 1418 AD, respectively, for sample H2.

5. Emergence estimated from fossilized assemblages

Fossilized assemblages were observed at elevations from approximately 0.3 to 1.6 m. A single elevation was observed for the fossilized assemblages at Sites A, B, D, and E, whereas those at Sites C, F, G, and H were continuously distributed over elevation

ranges. In addition, an upper assemblage (samples C1 and C2) and a lower assemblage (sample C3) were observed at Site C. For the assemblages with continuous distributions, we took samples from both the top and the bottom to measure the dates. The thicknesses of the assemblages were up to approximately 1 cm. Thus, we did not consider a date variation in the thickness direction.

The ages of the samples, as determined by the ^{14}C method, are summarized in Table 1. Figure 4a shows the relationships between the ages calibrated by the ^{14}C method and the observed elevations.

We obtained dates of approximately 1200–1300 AD for samples B1, C1, D1, E1, F1, and H1; approximately 1400 AD for samples F2 and H2; approximately 1500–1600 AD for samples A1, B2, C2, and G1; and approximately 1800 AD for samples C3 and G2.

The vertical change in the intertidal sessile organisms (h_{change}) was estimated from the elevations of the intertidal sessile organisms ($h_{observe}$) by subtracting the paleo-sea level at the date of each fossil ($h_{sea\text{-}level}$) and the elevation of the modern upper-growth limit ($h_{correct}$). We selected the modern assemblage of Site I (elevation 0.58 m), which is located at the highest elevation among the modern assemblages in the study area, as the elevation of the modern upper-growth limit. There are no reports of uplift around Site I, although the 1993 Noto Hanto-oki earthquake occurred around the northern part of the Suzu-oki segment.

For the reasons mentioned above, we estimated the vertical change (h_{change}) of the intertidal sessile organisms using the following formula:

$$h_{change} = h_{observe} - h_{sea\text{-}level} - h_{correct}$$

Figure 4b shows the calibrated ages (medians) and vertical changes of the samples.

We have two or three samples from Sites B, C, F, G, and H. These show vertical changes of 0.05 m for samples B1 and B2, 0.16 m for samples C1 and C2, 0.17 m for

samples F1 and F2, and 0.14 m for samples H1 and H2, 0.63 m for samples C2 and C3, and 0.26 m for samples G1 and G2. Thus, the differences in the vertical changes between samples C2 and C3 and between samples G1 and G2 are greater than 0.2 m. Considering that the height of the *P. kraussii* habitat is approximately 0.2 m, the difference in the vertical change at site C in particular is obviously significant. We estimated that the uplift occurred between the latest year at which the vertical change was recognized and the oldest year at which the vertical change was not recognized. We therefore infer that an earthquake that occurred between 1600 and 1800 AD caused the uplift. The vertical changes in samples B1, C1, F1, and H1 were greater than those in samples B2, C2, F2, and H2, respectively. Samples B1, C1, F1, and H1 date from before 1280 AD, and samples B2, C2, F2, and H2 date from after 1420 AD. There is a possibility that another earthquake occurred between 1280 and 1420 AD, but the differences between the samples is sufficient to explain the influence of the width of the *P. kraussii* habitat and the change in the local sea level.

6. Fault modeling for topographic analysis

Figure 5a shows the distribution of the vertical displacements along the northern coast of the Noto Peninsula. We neglected samples C3 and G2, which we dated to later than 1800, because we were focused on constructing a fault model of the event that occurred between 1600 and 1800. The distribution shows no uplift at Sites A and B, the largest displacement (approximately 0.8 m) at Site C (samples C1 and C2), and a gradual decrease from Sites C to H. This uplift area corresponds to the hanging-wall side of the Wajima-oki segment and is located over a range of 20 km from Sites C to G. Furthermore, there are no reports of inland active faults in this area (Fig. 1). These facts suggest that the Wajima-oki segment was the probable source fault of the event that

uplifted the coastal area from Sites C to G between 1600 and 1800. We excluded Site H from the modeling because it may have been affected by the activity of the Suzu-oki segment.

To calculate the displacements, we considered simple rectangular faults in a homogenous elastic half-space (Okada, 1992). For simplicity, following the fault model of the 2007 Noto Hanto earthquake that ruptured the eastern half of the Monzen-oki segment (Awata et al., 2008; Hiramatsu et al., 2008), we fixed the values of several fault parameters: the dip was set to be 60°, the depth of the upper fault end was set to be 2 km, and the depth of the lower fault end was set to be 15 km. We set the location of the fault based on the fault trace of the Wajima-oki segment (Inoue and Okamura, 2010). In the western part of the Wajima-oki segment, two faults extend parallel to each other. The fault model along the southern trace yielded a better fit to our observations than that along the northern trace. Thus, the strike and the total length of the fault were set to 62° and 23 km, respectively, based on the southern trace. We divided the fault into three sections: the western fault plane (fault A, length 8.7 km), the central fault plane (fault B, length 8.0 km), and the eastern fault plane (fault C, length 6.4 km), based on the geometry of the fault (Fig. 5a). The estimated fault parameter values are listed in Table 2.

We used the nonlinear inversion method to search for the optimum net slip to the rake of the faults, 90°, 105°, 120°, and 135°, which is between 90° (a reverse fault) and 135° (the same as that of the 2007 Noto Hanto earthquake). We calculated coseismic crustal deformations for four cases of net slip: the same deformation for all sections (Case 1), the same deformation for the western and central sections (Case 2), the same deformation for the central and eastern sections (Case 3), and different deformations for each section (Case 4). We set as the zero point the elevation of the modern upper-growth

limit of Site I1.

Table 3 shows the results of the calculations, and Fig. 5a shows the distribution of the vertical displacements along the coastline for a rake R = 90°. Considering that the height of the *P. kraussii* habitat is approximately 0.2 m, the results for Cases 1 and 2 differ notably from the observations for Sites C, D, and E (Figure 5a). These large deviations mean that Cases 1 and 2 are inadequate to explain the distribution of the vertical displacements. Our inversion results show that the Akaike information criterion (AIC) value is at a minimum for Case 3 with a rake of 90°, a net slip of the western fault plane (fault A) of 1.8 m, and a net slip of the central and eastern fault planes (faults B and C) of 0.6 m and that Case 3 yields the best fit to the estimated vertical displacements. Figure 5b shows the distribution of the vertical displacement in the northern part of the Noto Peninsula for Case 3 with R = 90°. The values of AIC for Case 3 with R = 105° and those for Case 4 with R = 90° and 105° are equivalent to those for Case3 with R = 90°, and the difference in the AIC between them is less than two (Table 3). Therefore, we cannot present a unique fault model for the Wajima-oki segment to explain the estimated vertical displacements. However, based on our modeling, we can conclude that the most suitable fault model is a reverse fault or a reverse fault with right–lateral slip and contains a net slip of the western fault plane that is larger than those of the central and eastern fault planes.

7. Discussion

7.1. Comparison between the fault model and the 1729 earthquake

Usami (2003) assumed the seismic source of the 1729 earthquake based on the distribution of collapsed buildings (Fig. 5b), although the source fault of this event has not been identified. The magnitude of this earthquake (comparable to the JMA

magnitude (M_{JAM})) has been estimated empirically to be 6.6–7.0, based on the area of the damaged zones (Usami, 2003). We discuss here relationships between the fault model described in the previous section and the 1729 earthquake.

There are no other reports of the occurrence of a large earthquake that would have caused coastal uplift in this area after 1600. The temporal overlap between the 1729 earthquake and the uplift event that occurred between 1600 and 1800 therefore suggests strongly that the coastal uplift estimated from the distribution of the vertical displacement of the fossilized *P. kraussii* was caused by the 1729 earthquake.

Our inversion result shows that a rake of 90°, a net slip of the western fault plane of 1.8 m, and a net slip of the central and eastern fault planes of 0.6 m provide the best fit to the estimated vertical displacements. The calculation results show that the range of the uplift area greater than 0.2 m associated with the reverse faulting of the Wajima-oki segment extends 10 km from coast to inland (Fig. 5b). The area above the fault plane roughly matches the distribution of the collapsed building ratios of the 1729 earthquake, and the points indicating high collapse ratios tend to be distributed over the area above the western fault plane that has a larger net slip (Fig. 5b). Thus, the spatial relationship between the uplift area and the zone damaged by the 1729 earthquake supports the premise that the 1729 earthquake caused the coastal uplift. The moment magnitude (Mw) calculated from the fault model for topographic analysis, assuming a rigidity of 30 GPa (e.g., Hiramatsu et al., 2008), is 6.6, which corresponds to the JMA magnitude (M_{JMA}) of 6.9, using the formula proposed by Takemura (1998):

$$\log M_0 \text{ (dyne • cm)} = 1.2\, M_{JMA} + 17.7$$

where M_0 is the seismic moment. This is consistent with the magnitude range of 6.6–7.0 estimated empirically from the area of the zones damaged by the 1729 earthquake (Usami 2003).

For the reasons mentioned above, we conclude that the estimated vertical displacement from the distribution of *P. kraussii* was caused by the fault movement of the Wajima-oki segment; that is, that the Wajima-oki segment was the source fault of the 1729 event.

7.2. Activity of the Wajima-oki segment during the Late Pleistocene

Inoue and Okamura (2010) reported that clear faults of the Wajima-oki segment displaced erosional surfaces dating from the last glacial age, with displacements of up to 10 m. As a result of measurement of the difference in the erosional surface at the last glacial age reported by Inoue and Okamura (2010), a maximum gap was found at the line N20, which is located at the eastern end of the western fault plane (fault A) (Fig. 6b). The gap decreases gradually with increasing distance from the line N20, and there is no gap at the eastern fault plane (fault C). The distribution pattern of the gap is similar to that of the net slips of our fault model: the western net slip is larger than the central and eastern net slips and is similar to that of the vertical displacement calculated for Case 3.

The marine terraces corresponding to MIS5e (125 ka) have a distribution extending from Site B to near Site D and locally at Site G, whereas no marine terraces have been reported from the east of Site D to near Site G (Ota and Hirakawa, 1979; Koike and Machida, 2001) (Fig. 6a).

The vertical displacement caused by the activity of the Wajima-oki segment in 1729, as described in the previous sections, decreases from Sites C to H, although the former shoreline on the marine terraces shows that the elevation rises from Site C (approximately 50 m) to near Site D (approximately 80 m) (Fig. 6b). The altitudinal distribution of the former shoreline from Sites C to D does not seem to coincide with the vertical displacement caused by the 1729 earthquake and the distribution of the

erosional surface at the last glacial age, according to the seismic survey.

This discrepancy implies that the long-term average of the fault movement of the Wajima-oki segment may differ from the fault movement of the 1729 earthquake estimated in this study or that the fault movement of the adjacent segment may have contributed to the altitudinal distribution of the former shoreline. Another plausible cause of the discrepancy is multiple ruptures involving adjacent segments. However, there are no reports to support this hypothesis. According to Hiramatsu et al. (2008), the elevation distribution of MIS5e marine terraces on the northwestern coast of the Noto Peninsula suggests the possibility of the existence of a long-term aseismic uplift, based on comparison of considerable coseismic uplifts caused by active faults off the northwestern coast. If the same process occurred along the northern coast of the Noto Peninsula, the difference mentioned above may have been caused by a long-term aseismic uplift. To understand the reason for the discrepancy, it is important to reexamine the distributions of marine terraces.

8. Conclusions

We investigated the vertical changes along the northern coast (≥ 60 km in length) of the Noto Peninsula, where active reverse faults are distributed on the seafloor off the coast. We used intertidal sessile organisms as markers of the vertical changes. The vertical changes estimated from the elevations and ages of the intertidal sessile organisms reveal that coastal emergence occurred between 1600 and 1800. We constructed a fault model for the Wajima-oki segment with a moment magnitude of 6.6 to explain the distribution of the vertical displacements along the coast. Only one damaging earthquake, which occurred in 1729, has been reported for this area. The date of the coseismic crustal deformation is consistent with the date of the 1729 earthquake

occurrence. This coincidence, together with the correspondence between the estimated uplift area and the area damaged by the 1729 earthquake, leads us to conclude that the latest seismic event of the Wajima-oki segment was the 1729 earthquake.

Acknowledgments

For the fault modeling conducted in this study, we used an inversion code provided by Takuya Nishimura at the Research Center for Earthquake Prediction of the Disaster Prevention Research Institute, Kyoto University. We used Generic Mapping Tools (Wessel and Smith, 1998) to produce Figures 1 and 5b. We used the Red Relief Image Map at 1-m DEM resolution (Asia Air Survey Co., Ltd., Japanese patent publication No. 3670274) to produce Figures 3a–i. Constructive comments by Rob Witter and an anonymous reviewer are appreciated.

References

Awata, Y., Toda, S., Kaneda, H., Azuma, T., Horikawa, H., Shishikura, M., Echigo, T., 2008. Coastal deformation associated with the 2007 Noto Hanto earthquake, central Japan, estimated from uplifted and subsided intertidal organisms. Earth Planet. Space 60, 1059–1062.

Bronk Ramsey, C., 2009. Bayesian analysis of radiocarbon dates. Radiocarbon 51(1), 337–360.

Grinsted, A., Moore, J. C., Jevrejeva, S., 2009. Reconstructing sea level from paleo and projected temperatures 200 to 2100 AD. Clim. Dyn. doi:10.1007/s00382-008-0507-2.

Hiramatsu, Y., Moriya, K., Kamiya, T., Kato, M., Nishimura, T., 2008. Fault model of the 2007 Noto Hanto earthquake estimated from coseismic deformation obtained

by the distribution of littoral organisms and GPS: Implication for neotectonics in the northwestern Noto Peninsula. Earth Planet. Space 60, 903–913.

Hsieh, M. L. Rau, R. J., 2009. Late Holocene coseismic uplift on the Hua-tung coast, eastern Taiwan: Evidence from mass mortality of intertidal organisms. Tectonophysics 474, 595–609. doi:10.1016/j.tecto.2009.04.031.

Imajima, M., 1979. A guide to identification of principal fouling organisms (1) Tube worms. Marine Fouling 1(1), 29–35.

Inoue, T. Okamura, Y., 2010. Digital Geological Map. Geological Survey of Japan AIST, S-1.

Katagawa, H., Hamada, M., Yoshida, S., Kadosawa, H., Mitsuhashi, A., Kono, Y., Kinugasa, Y., 2005. Geological development of the east sea area of the Noto Peninsula district in the Neogene Tertiary to Quaternary, central Japan. J. Geogr., 114, 791–810 (in Japanese with English abstract).

Kayanne, H., Yamamuro, M., Matsumoto, E., 1987. Pomatoleios kraussii (BAIRD) as a paleo sea level indicator on the southeast coast of Boso Peninsula, central Japan. Quaternary Research 26(1), 47–57.

Koike, K. Machida, H., 2001. Atlas of Quaternary Marine Terraces in the Japanese Islands. Univ. of Tokyo Press, Tokyo.

Maemoku, H., 1988. Holocene crustal movement in Muroto Peninsula, southwest Japan. Geographical Review of Japan 61(10), 747–769.

Matsu'ura, M. Hasegawa, Y., 1987. A maximum likelihood approach to non-linear inversion under constraints. Phys. Earth Planet. Inter. 47, 179–187.

Miura, T. Kajihara, T., 1983. An ecological study of serpulid polychaetous annelids. Benthos Research 25, 40–45.

Miura, T., Kajihara, T., 1984. An ecological study of the life histories of two Japanese

serpulid worms, *Hydroides ezoensis* and *Pomatoleios kraussii*. In: P. A. Hutchings (Eds.), Proceedings of the First International Polychaete Conference, Sydney, Australia, Linnean Soc. of New South Wales, pp. 338–354.

Moberg, A., Sonechkin, D., Holmgren, K., Datsenko, N., Karlen, W., 2005. Highly variable Northern Hemisphere temperatures reconstructed from low- and high-resolution proxy data. Letters to Nature 433, 613–617.

National Research Institute for Earth Science and Disaster Prevention (NIED), 2007. Earthquake mechanism information. http://www.hinet.bosai.go.jp/topics/noto070325/ (Last accessed, 3 August, 2015).

Nishihata, M., Yamamuro, M., Kayanne, H., 1988. Pomatoleios kraussii (BAIRD) and bench as paleo sea-level indicators on the west and south coast of Miura Peninsula, central Japan. Quaternary Research 27(1), 31–38.

Nohara, K., Noguchi, T., Anada, F., Hamada, M., Onoda, S., Numata, Y., Yamano, Y., Suzuki, Y., Sato, H., 2007. The crustal deformation associated with the 2007 Noto Hanto earthquake studied using airborne LiDAR. Bull. Earthquake Res. Inst. Univ. Tokyo 82, 321–331.

Okada, Y., 1992. Internal deformation due to shear and tensile faults in a half-space. Bull. Seismol. Soc. Am. 82, 1018–1040.

Okamura, Y., 2002. Explanatory Notes of Geological Map East of Noto Peninsula, Marine Geology Map Series 59 (CD). Geol. Surv. Jpn., Tsukuba.

Ota, Y., Hirakawa, K., 1979. Marine terraces and their deformation in Noto Peninsula, Japan Sea side of central Japan. Geogr. Rev. Jpn. 52, 169–189 (in Japanese with English abstract).

Ozaki, M., 2010. 1:200,000 Geological map of the northern part of Noto Peninsula. Digital Geoscience Map S-1.

Ozawa, S., Yarai, H., Tobita, M., Une, H., Nishimura, T., 2008. Crustal deformation associated with the Noto Hanto earthquake in 2007 in Japan. Earth Planet. Space 60, 95–98.

Ramos, N. T. Tsutsumi, H., 2010. Evidence of large prehistoric offshore earthquakes deduced from uplifted Holocene marine terraces in Pangasinan Province, Luzon Island, Philippines. Tectonophysics 495, 145–158. doi:10.1016/j.tecto.2010.08.007.

Reimer, P., Baillie, M. G. L., Bard, E., Bayliss, A., Beck, J. W., Blackwell, P. G., Bronk Ramsey, C., Buck, C. E., Burr, G. S., Edwards, R. L., Friedrich, M., Grootes, P. M., Guilderson, T. P., Hajdas, I., Heaton, T. J., Hogg, A. G., Hughen, K. A., Kaiser, K. F., Kromer, B., McCormac, F. G., Manning, S. W., Reimer, R. W., Richards, D. A., Southon, J. R., Talamo, S., Turney, C. S. M., van der Plicht, J., Weyhenmeyer, C. E., 2009. IntCal09 and Marine09 radiocarbon age calibration curves, 0–50,000 years cal BP. Radiocarbon 51(4), 1111–1150.

Research Group for Active Fault of Japan (RGAFJ), 1991. Active Fault in Japan– Sheet Maps and Inventories (revised edition). University of Tokyo Press, Tokyo, 437 pages (in Japanese with English summary).

Sakai, S., Kato, A., Iidaka, T., Iwasaki, T., Kurashimo, E., Igarashi, T., Hirata, N., Kanazawa, T., the Group for the Joint Aftershock Observation of the 2007 Noto Hanto Earthquake, 2008. Highly resolved distribution of aftershocks of the 2007 Noto Hanto earthquake by a dense seismic observation. Earth Planet. Space 60, 83–88.

Sato, H., Iwasaki, T., Kanazawa, T., Miyazaki, S., Kato, N., Sakai, S., Yamada, T., Miyauchi, T., Ito, T., Hirata, N., 2007. Characterization of the 2007 Noto Hanto earthquake, central Japan: Insights from seismic profiling, aftershock observations,

and co-seismic crustal deformation. Bull. Earthquake Res. Inst. Univ. Tokyo 82, 369–379.

Shishikura, M., Echigo, T., Maemoku, H., Ishiyama, T., Nagai, A., 2008. Uplifted sessile assemblages on the southern coast of the Kii Peninsula, related to historical earthquakes along the Nankai Trough. Historical Earthquakes 23, 21–26.

Shishikura, M., Echigo, T., Namegaya, Y., 2009. Evidence for coseismic and aseismic uplift in the last 1000 years in the focal area of a shallow thrust earthquake on the Noto Peninsula, west-central Japan. Geophys. Res. Lett. 36, L02307, doi:10.1029/2008GL036252.

Takemura, M., 1998. Scaling law for Japanese intraplate earthquake in special relations to the surface and the damages. Zisin Second Series 51, 211–228.

Usami, T., 2003. Materials for Comprehensive List of Destructive Earthquakes in Japan. [416] – 2001 [Latest Edition], Univ. of Tokyo Press, Tokyo.

Wessel, P., Smith, W. H. F., 1998. New, improved version of the Generic Mapping Tools released. EOS Trans. AGU 79, 579.

Yamaguchi, M., Ota, Y., 2004. Tectonic interpretations of Holocene marine terraces, east coast of Coastal Range, Taiwan. Quaternary International 115–116, 71–81.

Figures and tables

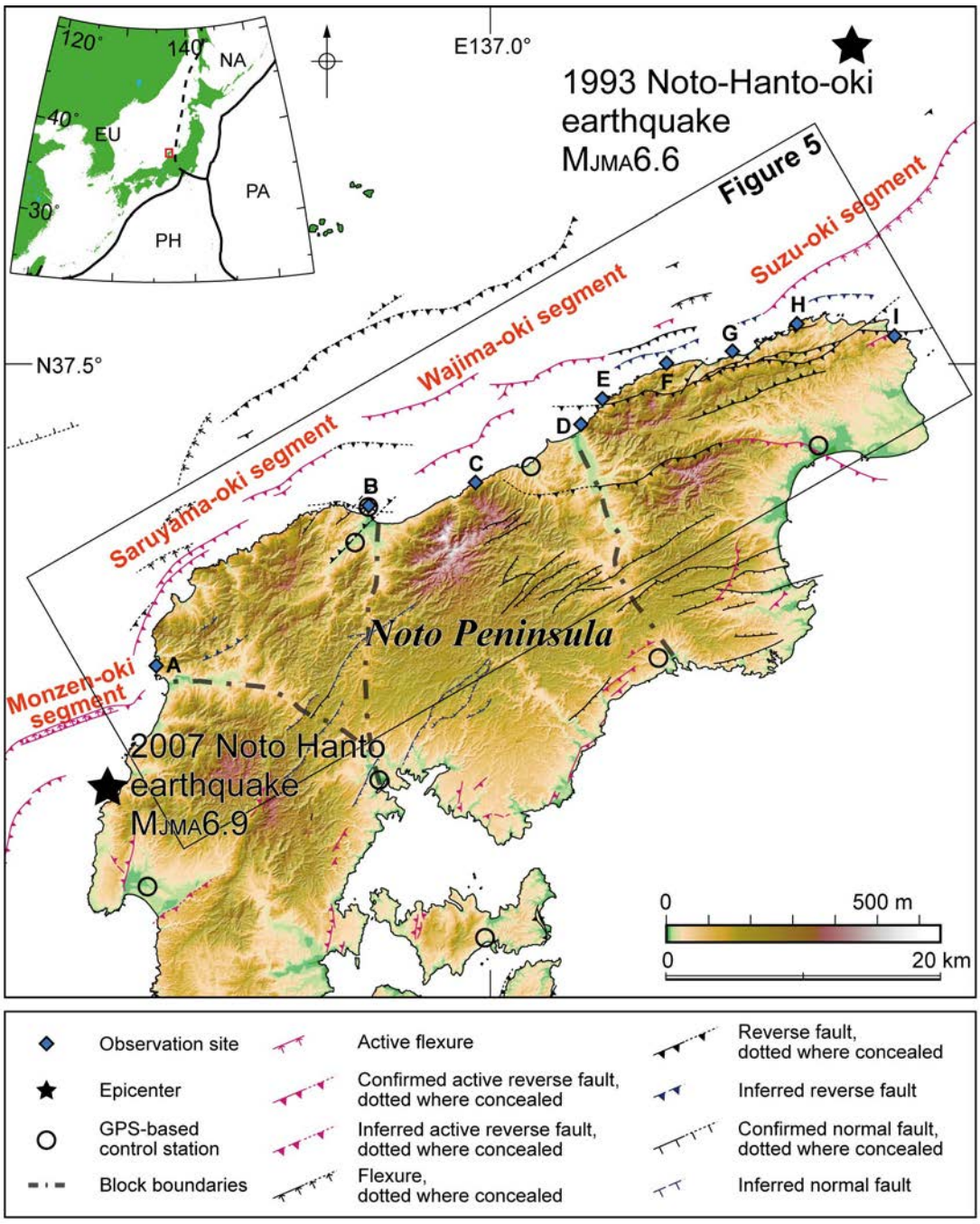

Fig. 1. Topographic map of the Noto Peninsula, showing locations of survey sites considered in this study (diamonds) and active reverse faults (barbs pointing downward) located offshore (Inoue and Okamura, 2010) and on land of the northern Noto Peninsula. Dotted-and-dashed lines indicate the block boundaries reported by Ota and Hirakawa (1979). The rectangle indicates the area shown in Figure 5. (Inset map) EU: Eurasian

Figure is color.

plate, NA: North American plate, PH: Philippine plate, PA: Pacific plate.

Fig. 2. Photo of fossilized *P. kraussii* assemblages on a rocky coast (Site C). The white arrows in (a) indicate modern intertidal sessile organisms such as *P. kraussii* (elevation 0.15–0.36 m). The black arrows in (b) indicate fossilized assemblages (Sample C1, elevation 1.59 m) in the red square in (a). The scale is 0.2 m.

Figure is color.

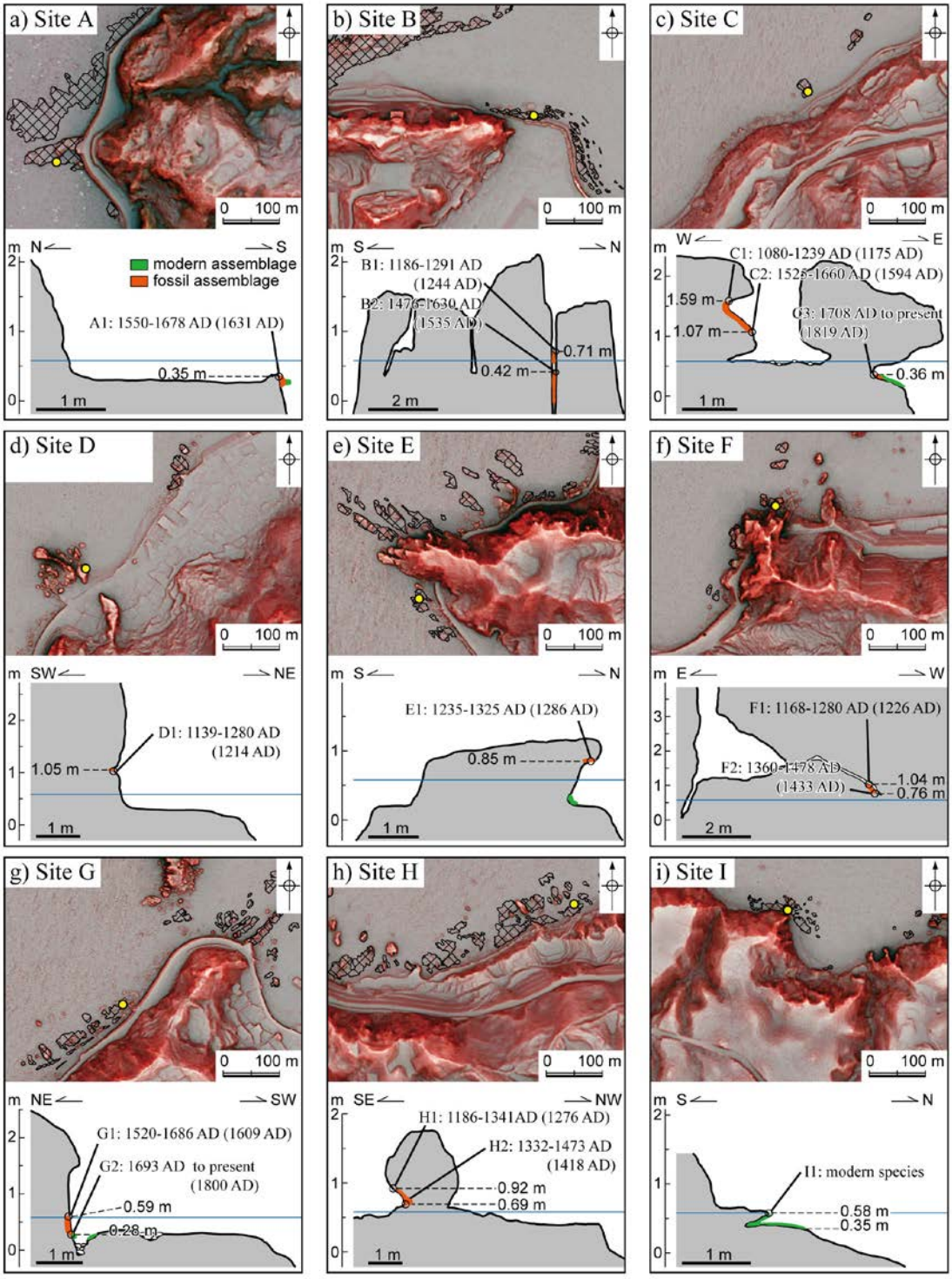

Fig. 3. (a)–(i) Microtopography (upper panel) and topographic profile (lower panel) of each site. The zero point of the vertical axis is the mean sea level of Tokyo Bay. The yellow circle in the upper panel shows the sampling point. The topography is represented by the Red Relief Image Map at 1-m DEM resolution (Asia Air Survey Co.,

Ltd.). The diagonal grid shadings in the upper panel indicate wave-cut benches distributed in the basal portion of a wave-cut cliff. The blue line in the profile indicates the elevation of modern upper-growth limit at Site I, which was used as the reference elevation for estimation of vertical displacements.

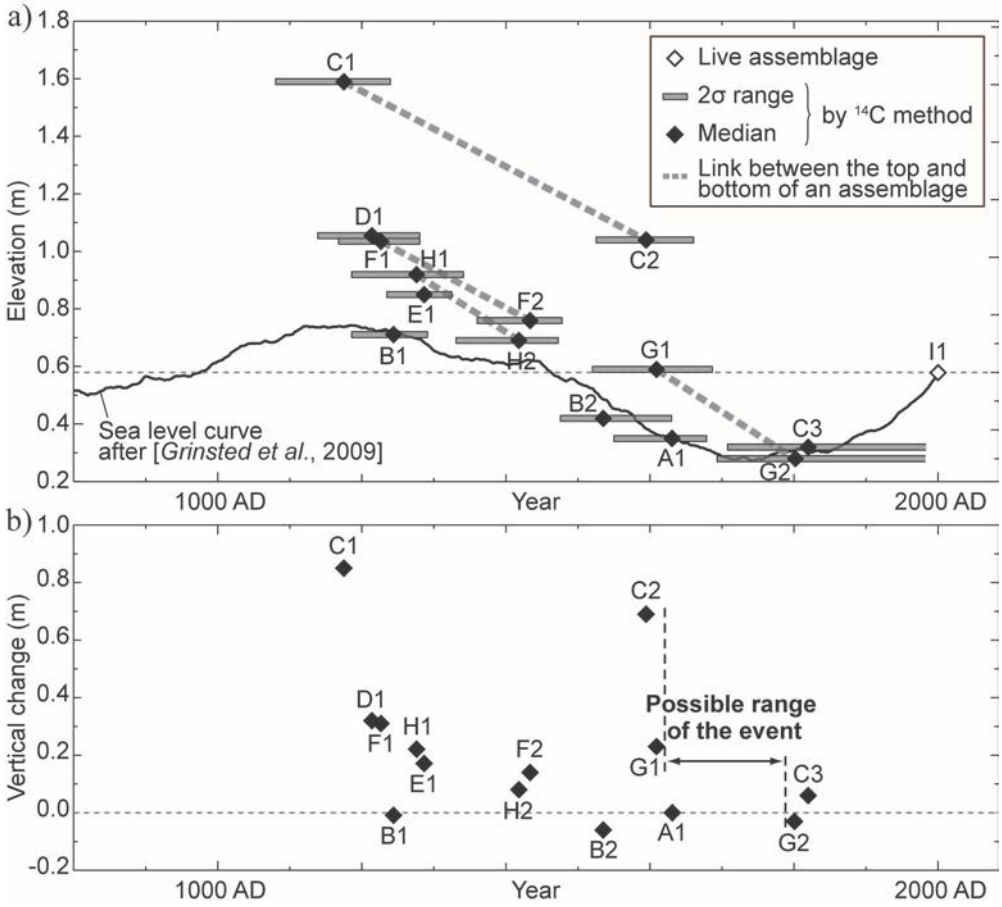

Fig. 4. (a) Relationship between observed elevations, calibrated ages estimated using the ^{14}C method, and the sea level change curve (Grinsted et al., 2009). The zero point of the sea level change curve was calibrated with respect to the elevation of the modern upper-growth limit (Sample I1, elevation 0.58 m). (b) Plot of the vertical changes versus the calibrated ages (Table 1).

Figure is black-and-white.

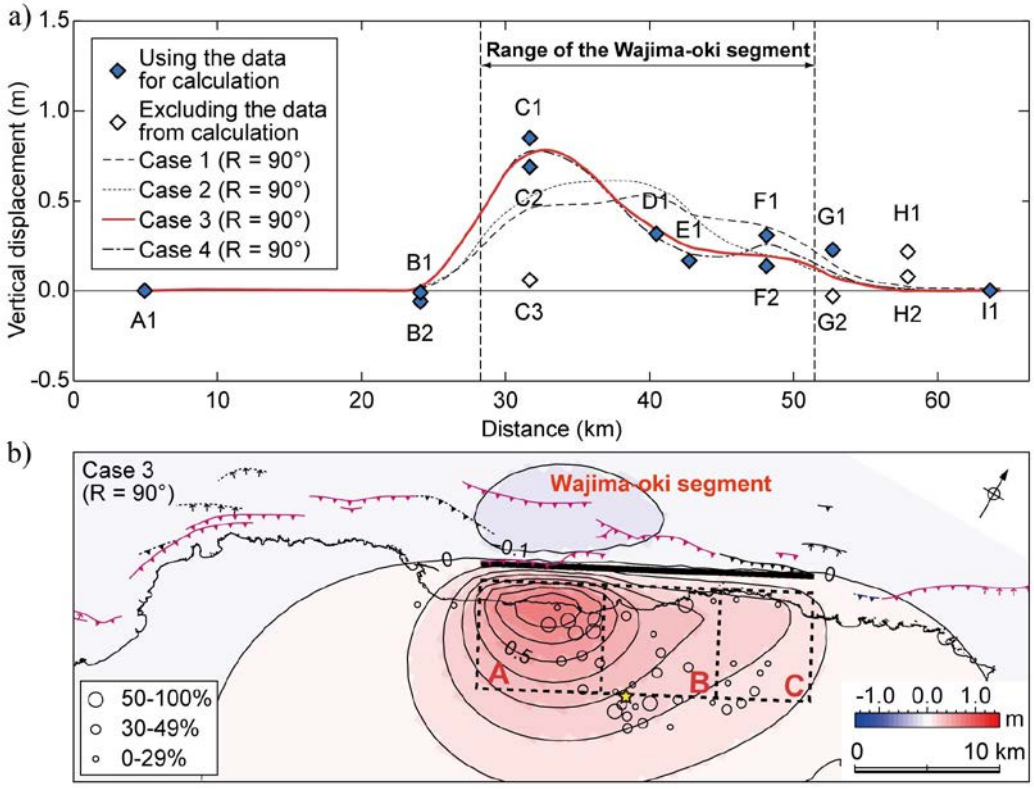

Fig. 5. (a) Distribution of the vertical displacements estimated in this study (diamonds) and those calculated using a fault model (dashed line). (b) Location of the fault model (black dotted rectangle with a solid line as the upper edge) and the distribution of the vertical displacements (contour lines) calculated from the fault model. The contour interval is 0.1 m. The black circles indicate the percentage of collapsed buildings as a result of the 1729 earthquake (Usami, 2003). The yellow star is the epicenter of the 1729 earthquake as estimated by Usami (2003) from the distribution of collapsed building ratios.

Figure is color.

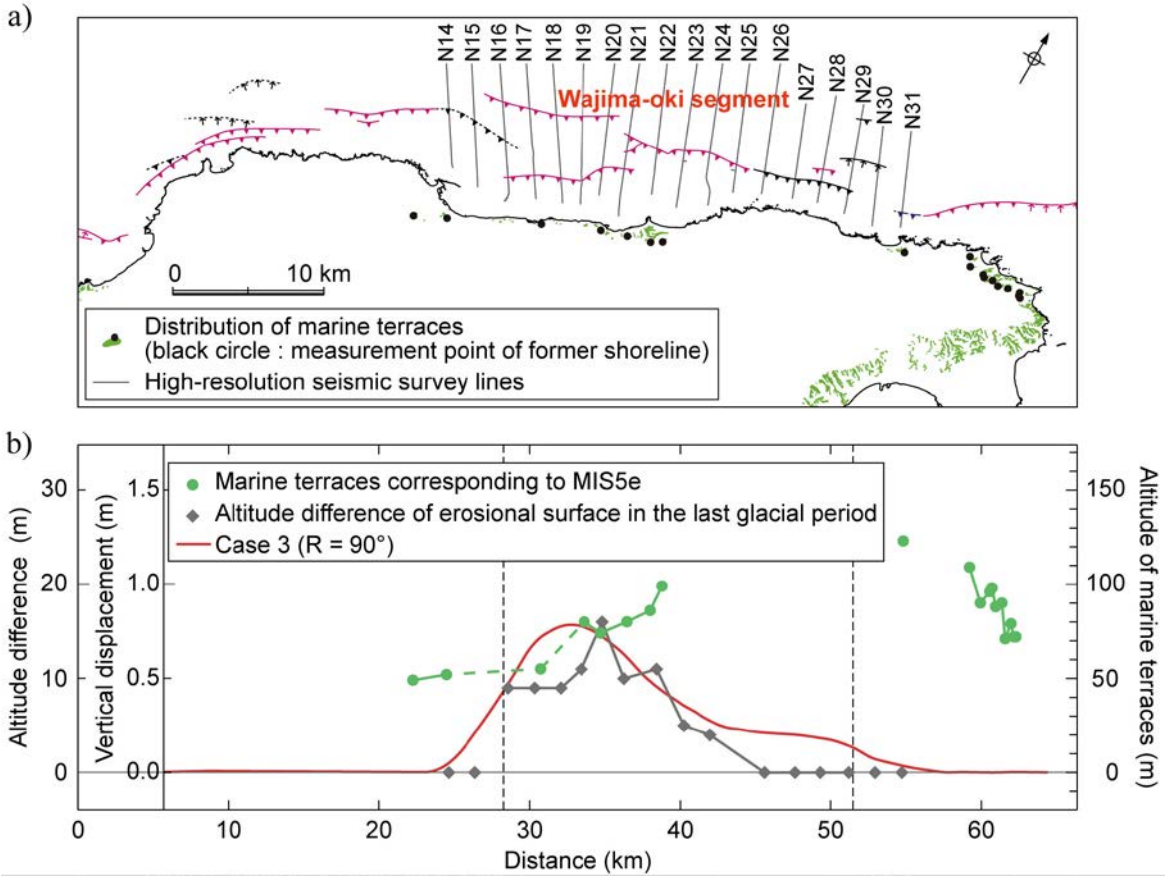

Fig. 6. (a) Distribution map of marine terraces corresponding to MIS5e (Koike and Machida, 2001) and the locations of high-resolution seismic survey lines (Inoue and Okamura, 2010). Only the former shoreline of marine terraces facing the northern coast of the Noto Peninsula was selected. (b) Distribution of the altitude differences of the erosional surface in the last glacial period (black diamonds) and the coastal uplift calculated for Case 3 using the fault model (red line).

Figure is color.

Table 1

Summary of the radiocarbon dates and elevations of the samples in this study.

	Radiocarbon dates					Elevation [a]		
Sample no.	$\delta^{13}C$ (‰)	^{14}C age (yrBP)	Calibrated age 2σ (cal AD)	Median (cal AD)	Laboratory code	$h_{observe}$ (m)	$h_{sea\text{-}level}$ (m)	h_{change} (m)
A1	4.41	679 ± 19	1550–1678	1631	IAAA-103858	0.35	-0.23	0.00
B1	1.14	1169 ± 20	1186–1291	1244	IAAA-111189	0.71	0.14	-0.01
B2	-0.05	767 ± 24	1476–1630	1535	IAAA-103861	0.42	-0.10	-0.06
C1	1.50	1239 ± 20	1080–1239	1175	IAAA-111188	1.59	0.16	0.85
C2	8.51	713 ± 22	1525–1660	1594	IAAA-103806	1.07	-0.20	0.69
C3	2.36	507 ± 23	1708–...	1819	IAAA-103804	0.36	-0.28	0.06
D1	1.75	1202 ± 24	1139–1280	1214	IAAA-103803	1.05	0.15	0.32
E1	5.37	1109 ± 22	1235–1325	1286	IAAA-103802	0.85	0.10	0.17
F1	1.50	1190 ± 20	1168–1280	1226	IAAA-111187	1.04	0.15	0.31
F2	3.96	914 ± 23	1360–1478	1433	IAAA-110056	0.76	0.04	0.14
G1	1.10	690 ± 40	1520–1686	1609	Beta-279269	0.59	-0.22	0.23
G2	0.10	520 ± 40	1693–...	1800	Beta-279268	0.28	-0.27	-0.03
H1	2.30	1120 ± 40	1186–1341	1276	Beta-279267	0.92	0.12	0.22
H2	1.00	930 ± 40	1332–1473	1418	Beta-279266	0.69	0.03	0.08
I1	-	-	-	-		0.58	-	-

[a] $h_{observe}$: Observed elevation. $h_{sea\text{-}level}$: Estimated paleo-sea level. The value reflects the sea level at the time of the habitation when we measured using the sea level curve of Grinsted et al. (2009). h_{change}: Vertical change. The value is obtained by subtracting the estimated paleo-sea level and the elevation of the modern upper-growth limit (0.58 m) from the observed elevation.

Table 2

Fault parameters estimated in this study.

Depth (km)	Length (km)			Width (km)	Strike (deg)	Dip (deg)
	Western	Center	Eastern			
2.0	8.7	8.0	6.4	15.0	62	60

Table 3

Results of the nonlinear inversion method.

	Slip (m) (R = 90°)			AIC			
	Western	Center	Eastern	R = 90°	R = 105°	R = 120°	R = 135°
Case 1	1.0	1.0	1.0	92.7	91.9	91.2	90.6
Case 2	1.2	1.2	0.5	92.9	92.1	91.4	90.8
Case 3	1.8	0.6	0.6	77.0	78.3	79.8	82.0
Case 4	1.8	0.4	0.8	77.1	78.8	80.8	83.4